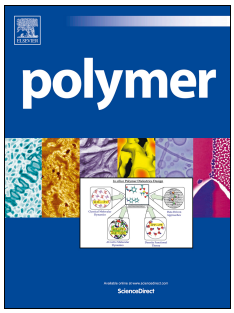

Molecular dynamics study of the shock response of polyurea✶

M. Manav, M. Ortiz

PII: S0032-3861(20)30934-4

DOI: https://doi.org/10.1016/j.polymer.2020.123109

Reference: JPOL 123109

To appear in: *Polymer*

Received Date: 7 August 2020

Revised Date: 23 September 2020

Accepted Date: 30 September 2020

Please cite this article as: Manav M, Ortiz M, Molecular dynamics study of the shock response of polyurea✶, *Polymer*, https://doi.org/10.1016/j.polymer.2020.123109.

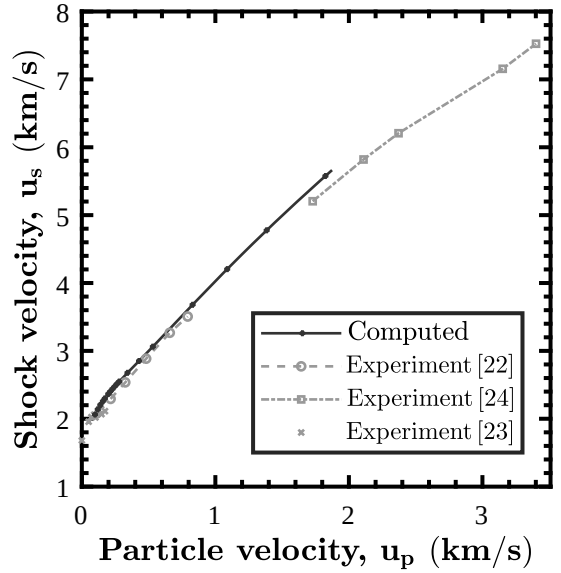
Shock velocity, u_s (km/s)
Particle velocity, u_p (km/s)
Computed
Experiment [22]
Experiment [24]
Experiment [23]

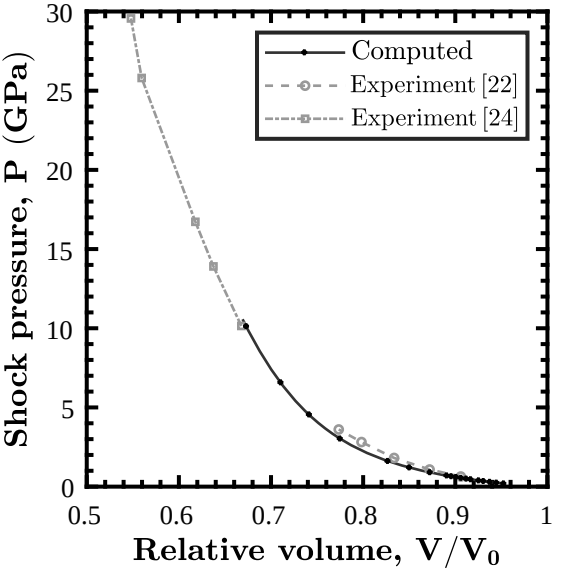
Shock pressure, P (GPa)
Relative volume, V/V_0
Computed
Experiment [22]
Experiment [24]

[orcid=0000-0002-8498-4144]
[orcid=0000-0001-5877-4824]

Molecular dynamics study of the shock response of polyurea*

M. Manav[a,*], M. Ortiz[a,**]

[a]California Institute of Technology, 1200 E California Blvd, Pasadena, CA 91125, USA

ARTICLE INFO

Keywords:
thermoplastic elastomers
polyurea
shock response
molecular dynamics

ABSTRACT

We leverage the phase segregated microstructure of polyurea to study its shock response using molecular dynamics (MD) simulation. The two phase segregated domains, the hard and the soft domains, are investigated separately. The shock response of the domains is studied using a multiscale shock-simulation approach that allows simulation of shocks at low shock pressures. Both domains exhibit an unconventional behavior at low shock velocities that is typically associated with polymers. The shock response of the hard domain is marked by energy dissipation due to hydrogen bond breaking. Moreover, the radial distribution function suggests a severe distortion in the ring structure of aromatic moieties in the hard domain at high shock pressure. Finally, the shock Hugoniot of polyurea, obtained by combining the response of the two domains using a mixing rule, shows excellent match with experimental data.

1. Introduction

Polyurea [1] is a thermoplastic elastomer (TPE) possessing remarkable mechanical and chemical resistance. Its molecular scale features and hierarchical microstructure endow it with exceptional shock and ballistic resistance [2–4], enabling its use as a blast protection coating for strategic installations, vehicles, bulletproof vests and helmets, and other applications [5–8]. In recent years, the molecular-level and mesoscale mechanisms responsible for shock and impact mitigation in polyurea have attracted considerable attention [4, 9], but remain to be completely understood.

A polyurea molecule is a multiblock copolymer with alternate arrangement of flexible aliphatic segments (from polyamine) and stiff aromatic moieties, Figure 1. In polyureas with long flexible segments (for example, the 'polyurea P1000 studied in this work), thermodynamic incompatibility results in a phase-segregated microstructure. Hard segments separate from soft segments and form ribbon-like hard domains (glassy due to a high glass transition temperature (T_g)) dispersed in a soft domain matrix (rubbery due to a low T_g) [10–15]. The hard domains act as stiffeners, as well as crosslinks between soft segments and, consequently, as constraints on their mobility near the interface, thereby modifying their dynamics [16]. In the hard domain, possible $\pi - \pi$ interactions between adjacent aromatic moieties and hydrogen bonds between the N − H group in urea and the O group in urea and ether [13] contribute to its rigidity. Atomic force microscopy (AFM) and small-angle X-ray scattering (SAXS) investigations of polyurea microstructure reveal that the width of the hard domain ribbons is $\sim 5 - 10$ nm and that two adjacent ribbons are separated by ≈ 7 nm [11, 13–15]. The aspect ratio of the ribbons is 20:1 or greater [17]. However, electron density variance estimation using SAXS integrated intensity in [13, 15] suggests that the boundaries between the hard and the soft domains are not sharp and considerable phase mixing is observed near the interface. This mixing can also be inferred from the clear discrepancy in distance between the two carbon atoms bonded to terminal aromatic rings of a hard segment ($\approx$ 3 nm) and the width of a hard domain ribbon. Furthermore, the experiments indicate that there is little or no crystallinity in polyurea [13, 15], which likely helps to improve shock energy absorption [18].

A number of experimental studies have been conducted with a view to characterizing and understanding the shock and impact properties of polyurea [2, 3, 19–24]. Polyurea exhibits strongly strain-rate dependent behavior and dissipates considerable energy [4]. Sarva *et al.* [19] studied the uniaxial compression stress-strain response of polyurea at strain rates varying from 10^{-3} s^{-1} to 10^{4} s^{-1}. They found a transition from rubbery behavior at low strain rates to leathery behavior at high strain rates. The exceptional shear resistance (500 MPa) of polyurea at high strain rates (10^{6} s^{-1}) and pressures (9 GPa) was found to match or even exceed that of high strength steels [3]. The impact resistance and shock resistance of polyurea have been argued to have differing underlying mechanisms. The impact resistance of polyurea emanates primarily from the impact energy absorbed in rubber-to-glass transition in the soft domain [2]. Bogoslovov *et al.* have compared the dielectric relaxation spectra of polybutadiene-based polyurea and polybutadiene rubber to find that a three-order-of-magnitude slower polybutadiene relaxation peak appears in polyurea. The time scale associated with this relaxation peak is close to the time scale of ballistic impact, promoting glass transition. Recently, Ransom *et al.* [25, 26] measured T_g of polyurea at different pressures using a diamond anvil cell and found that the glass transition in polyurea occurs at room temperature at 1.1 GPa pressure. Fragiadakis *et al.* [27] have shown that the ratio of hard and soft segments within a polyurea molecule has no significant effect on the glass transition or impact performance of polyurea, which is consistent with the idea that they are gov-

*We gratefully acknowledge support from the US Office of Naval Research, Naval Materials S&T Division, Dr. R. G. Barsoum manager, through grant N000141512453.

*Corresponding author
**Principal corresponding author
manav@caltech.edu (M. Manav); ortiz@caltech.edu (M. Ortiz)
http://ortiz.caltech.edu/ (M. Ortiz)
ORCID(s):

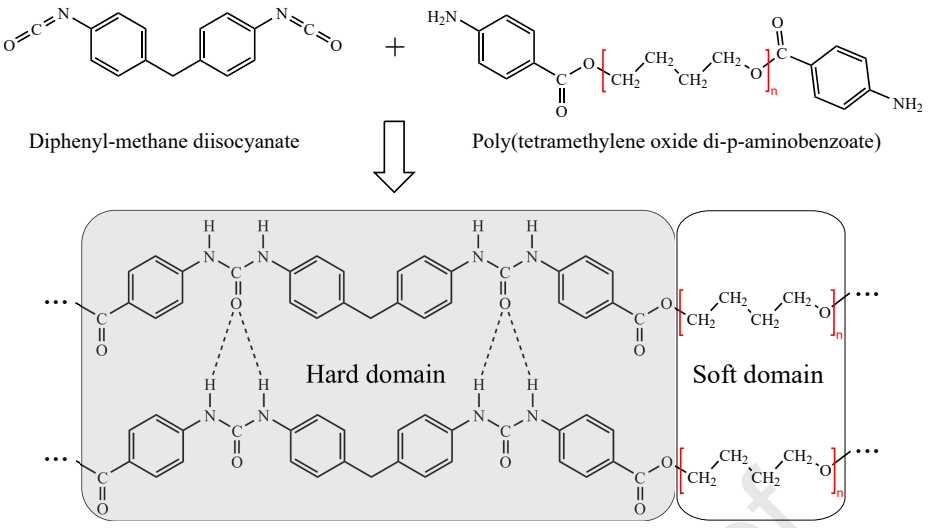

Figure 1: Synthesis of polyurea from reaction between a diisocyanate and a diamine. For polyurea P1000 studied here, n = 14.

erned by polymer segmental dynamics.

By contrast, the simulation studies of the shock response of polyurea indicate that the exceptional shock resistance of polyurea has origin in the hard domain [28]. Permanent densification, lateral atomic motion, and breaking and reformation of hydrogen bonds in urea linkages are thought to dissipate and disperse shock energy [28]. Shockwave capture and neutralization by a release wave moving faster than the shockwave has also been proposed as a shock attenuation mechanism in polyurea [29]. Densification in the hard domain is found to be crucial for that mechanism to operate. Qiao *et al.* [30] have speculated that, during deformation, the hard domains remain covalently linked through soft segments that act as a coupling link between the hard domains. Thus coupled hard domains undergo resonant motion during shock loading, resulting in energy trapping and enhanced dissipation.

Molecular dynamics modelling has also been undertaken to elucidate the dynamic response of polyurea [28, 31, 32]. This approach is made challenging primarily by two factors. Firstly, the time scale associated with phase-segregation is very long, making it computationally infeasible to obtain a phase-segregated microstructure in an all-atom (AA) simulation of polyurea. Secondly, the size of a domain ($\sim 5-10$ nm) is too large to be realistically represented in a representative volume element (RVE) of polyurea. To overcome these challenges, a coarse grained model can be adopted [31, 33, 34]. Another approach to overcome the first challenge in an AA polyurea simulation is to artificially group the hard-domain molecules together [28]. While the domain sizes in the RVE cannot reach representative values, it is argued in [32] that those model deficiencies do not affect the pressure-shear response of polyurea and a good agreement between simulation and experimental results is achieved.

In this work, leveraging the phase segregation in polyurea and following Heyden *et al.* [35], we study the shock response of the two domains independently and combine them to obtain shock Hugoniot of polyurea. This approach has threefold benefits. Firstly, it circumvents the limitations imposed by the long duration of simulations required to achieve phase segregation in an all-atom simulation of polyurea. Secondly, it obviates the need to consider simulation cells of > 10 nm size to have a representative RVE. Thirdly, it facilitates a comparative study of the shock response of the two domains. These advantages notwithstanding, the approach is limited to the calculation of the thermodynamic equilibrium properties of polyurea compressed by a shock wave, and does not elucidate the evolution and the structure of the shock wave. Furthermore, the mixed domain at the diffuse interface containing molecules from both the hard and the soft domains should ideally be considered as a separate domain. However, due to a lack of the experimental data on the mass fractions of the molecules from the hard and the soft domains in the mixed domain, and the mass fraction of the mixed domain in polyurea, it will not be considered separately.

We specifically perform molecular dynamics simulations of the two domains in polyurea P1000 independently. We begin by computing the glass transition temperature of the two domains. The results are similar to the values reported in literature after correcting for very high cooling rate in MD simulation, reinforcing confidence in the domain models. We then carry out multiscale shock simulations to obtain the shock Hugoniots of the two domains. We also investigate structural changes at the molecular scale due to shock pressure. Finally, the Hugoniots of the two domains are combined using an approach proposed by McQueen *et al.* [36] to obtain the shock Hugoniot of polyurea.

The paper is organized as follows. Section 2 describes the molecular dynamics model of the two domains, the multiscale shock simulations, and the mixing rule used to calculate the Hugoniot of polyurea from those of the hard and the soft domains. The shock response of the domains, shock-induced molecular-scale changes, and the Hugoniot of polyurea

are then described and discussed in Section 3. The paper ends with conclusions in Section 4.

2. Modelling

In this section, we develop molecular dynamics models of the two domains of polyurea. Then, multiscale shock simulations are used to characterize the shock Hugoniot of the domains. Finally, we apply McQueen's method to combine Hugoniot of the two domains and derive the Hugoniot of polyurea.

2.1. Molecular dynamics model

Figure 2 and Figure 3 show single molecules of the hard and the soft domains, respectively. We note that hard domain molecule contains all the phenyl rings and urea linkages up to the first aliphatic carbon in the soft domain. This arrangement is adopted in order to suppress the possibility of an artificial hydrogen bond formation if a hard domain molecule ends at the oxygen atom, as depicted in Figure 1. All the simulations were performed using LAMMPS [37] with the OPLS-AA force field [38, 39] and a time step size of 1 fs. The stress-strain relation for polyurea in uniaxial compression up to $\sim$ 8 GPa obtained from multiscale modeling employing OPLS-AA force field is shown in [35] to be in good agreement with experimental measurement, validating our choice of the force field. All NPT simulations used Nose-Hoover barostat and thermostat with thermal time constant of 100 fs and pressure time constant of 1000 fs.

For the hard domain simulations, Figure 2, a random configuration of 200 hard domain molecules placed in a simulation box with periodic boundary conditions at very low density was chosen as initial configuration. The configuration was initialized at 1 atm pressure and 800 K temperature, higher than the melting temperature of polyurea, and equilibrated for about 50 ns through an NPT simulation. A well-equilibrated configuration above melting temperature was cooled to 300 K at the cooling rate of 5 K/ns. On equilibrating the configuration at 300 K for 15 ns, it reached a target density of 1.1574 g/cm^3. The simulation box is of dimension 5.9 nm $\times$ 6.3 nm $\times$ 4.2 nm. Fast cooling suppresses crystal formation and produces an amorphous hard domain, as observed experimentally.

For the soft domain simulations, Figure 3, 100 soft domain molecules with appropriate end-to-end density distribution placed in a simulation box with periodic boundary condition at very low density defined the initial configuration. After equilibrating at 500 K temperature and 1 atm pressure for 50 ns, they were cooled down at a rate of 25 K/ns to 50 K. For shock simulations, a configuration at 300 K was equilibrated for 15 ns to reach a target density of 0.9265 g/cm^3. The dimensions of the simulation box were 5.5 nm $\times$ 6.8 nm $\times$ 4.8 nm. The increased cooling rate in comparison to the hard domain was introduced to prevent crystal formation. We observed very high degree of crystallization in the soft domain simulation cell at a 5 K/ns cooling rate and the resulting density at room temperature was comparable to that of high density polyethylene (HDPE).

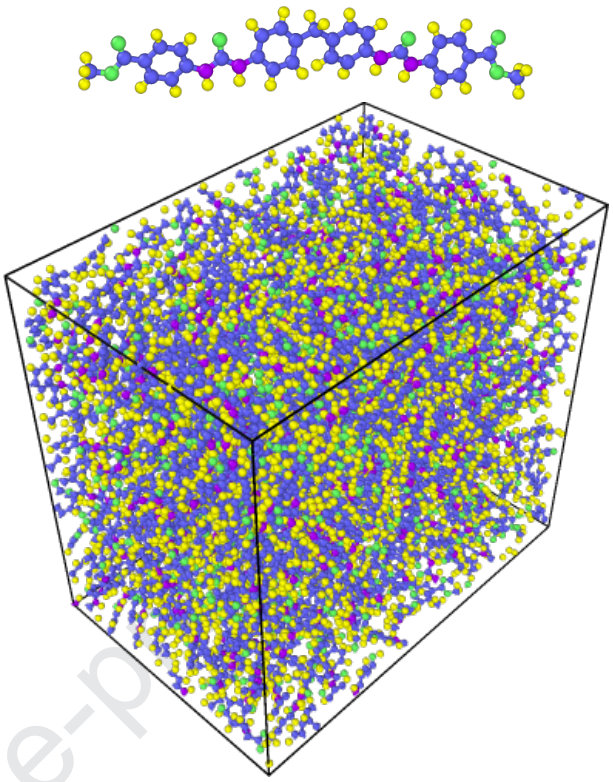

Figure 2: Hard domain single molecule and equilibrated configuration comprising 200 hard domain molecules.

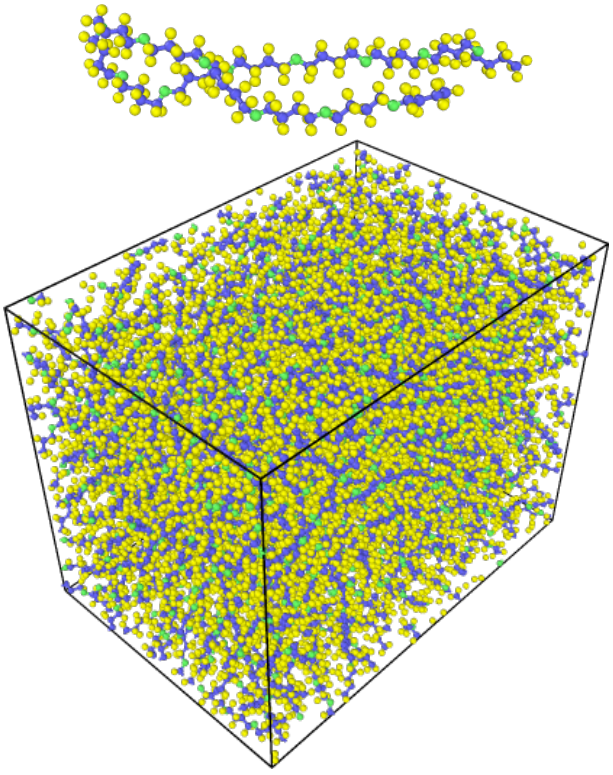

Figure 3: Soft domain single molecule and equilibrated configuration comprising 100 soft domain molecules.

The Hamiltonian of the systems is assumed to be of the form

$$\mathcal{H} = E_{pair} + E_{bond} + E_{angle} + E_{dihedral}, \tag{1}$$

where E_{pair}, E_{bond}, E_{angle}, and $E_{dihedral}$ are energies associated with pair interaction, bond extension, bending, and torsion, respectively. E_{pair} accounts for Pauli repulsion and van-der-Waals forces, modelled using a Lennard-Jones type potential U_{LJ}, and Coulombic interactions. The pairwise potential U_{LJ} is of the form

$$U_{LJ} = 4\epsilon\left(\left(\frac{r}{\sigma}\right)^{12} - \left(\frac{r}{\sigma}\right)^{6}\right) - U_{shift}, \tag{2}$$

with a cutoff distance (r_c) of 1 nm, where r is the interatomic distance. The potential is shifted by U_{shift} to ensure cutoff continuity. The Coulombic interaction potential between a pair of interacting atoms is

$$U_{coulomb} = \frac{q_1 q_2}{4\pi\epsilon_0 r}, \tag{3}$$

where ϵ_0 is the permittivity of vacuum. Long range Coulombic interactions were calculated using Ewald summation with a cutoff distance of 1 nm and a relative RMS error in per-atom electrostatic force of 10^{-4}. A harmonic approximation of the form

$$U_{bond} = K_{bond}(r - r_0)^2, \tag{4}$$

is used for potentials associated with bonds. Similarly, the angular potential is of the harmonic form

$$U_{angle} = K_{angle}(\theta - \theta_0)^2. \tag{5}$$

$E_{dihedral}$ is modeled using a Fourier potential

$$U_{dihedral} = \sum_{i=1,m} K_i(1 + \cos(n_i\phi - d_i)), \tag{6}$$

with $m = 3$, and n_i integers ≥ 0. This Hamiltonian has been used previously in MD simulations of polyurea [35].

2.2. Shock simulation in MD

The simulation of shocks in MD may be performed using nonequilibrium molecular dynamics (NEMD), whereby a long simulation cell is shocked at one end and its evolution is tracked. The simulations allow elucidation of the shock evolution, the structure of the shock front, and the thermodynamic state of the material behind the shock front. However, this approach is computationally expensive. Furthermore, low shock pressures are very challenging to simulate due to the prohibitively long simulation cell required to reach steady state. A number of multiscale shock simulation approaches have been proposed to improve computational efficiency [40–42]. They combine Rankine-Hugoniot equations with MD to evolve the material in a simulation cell to the thermodynamic state behind the shock front. The approaches do not require a large simulation cell and the shock Hugoniot can be determined at a much smaller computational cost than NEMD. However, the tradeoff is that the structure of the shock wave cannot be obtained.

In this work, we use the constant-stress Hugoniostat method proposed by Ravelo *et al.* [42], whereby a barostat, controlled by a strain-rate variable, compresses the simulation box at a finite rate to reach the prescribed shock pressure. An ergostat, controlled by a heat flow variable, uses the energy conservation equation in the Hugoniot relations and brings the energy of the simulation cell to its value at the shocked state. On choosing appropriate barostating, ergostating and damping parameters, the time evolution of temperature and pressure resembles that in NEMD simulation [42]. Therefore, plastic deformation and the final temperature are accurately captured by the method. The method also captures multiwave structures due to phase transitions. A shock pressure is prescribed and the simulation yields density of shocked material and temperature. Subsequently, shock and particle velocities are obtained using Hugoniot relations corresponding to mass and momentum conservation.

We refer to the pressure prescribed in the direction of shock propagation as the shock pressure and forgo specific mention of the direction of propagation. We have studied the shock response only up to a shock pressure of $\sim$ 10 GPa. In this range, the simulation results based on OPLS-AA force field is expected to be valid [35]. Also, we do not need to take into account the effects of disintegration of polymers at higher pressures, specifically ring polymers such as the molecules in the hard domain, which the current model is not equipped to capture. The disintegration appears as a transition in shock Hugoniot of polymers typically near $\sim$ 20 GPa shock pressure [43, 44].

2.3. Hugoniot of a mixture

The shock Hugoniot of the two domains obtained by the method just described can be combined to get the Hugoniot of polyurea. To this end, we use the approach proposed by McQueen *et al.* [36] to characterize the shock Hugoniot of mixtures. When a shock wave passes through a mixture, the pressure in different domains equilibrates. However, the equilibrium pressures occur at different internal energies and temperatures in different domains [45]. To account for this effect, McQueen *et al.* [36] proposed to first calculate the 0 K isotherm for each domain using the relation

$$\left(\frac{\partial P}{\partial v}\right)_{0\mathrm{K}} + \frac{\gamma_0}{v_0}P_{0\mathrm{K}} = \frac{\gamma_0}{2v_0}\left[P_H + \left(\frac{2v_0}{\gamma_0} + v - v_0\right)\left(\frac{\partial P}{\partial v}\right)_H\right], \tag{7}$$

where P, v, v_0, γ_0 are the pressure, specific volume, specific volume at zero pressure and Mie-Gruneisen parameter for the material at 0 K, respectively. Subscripts 0K and H denote values at 0 K temperature and along the Hugoniot curve, respectively. This relation is obtained using thermodynamic relations combined with the Mie-Gruneisen equation of state (EOS), and by assuming γ_0/v_0 to be a material constant independent of temperature and shock pressure.

The right-hand side of (7) for each domain is obtained from shock simulations. By solving (7), the 0 K isotherm for each domain is obtained. Then, at each pressure, the properties of the mixture are obtained using the mixing rule

$$v = \Sigma_i m_i v_i, \quad \frac{v_0}{\gamma_0} = \Sigma_i m_i \left(\frac{v_0}{\gamma_0}\right)_i, \quad \text{and} \quad E = \Sigma_i m_i E_i, \tag{8}$$

where m_i is the mass fraction of each domain, and summation is performed over each domain. This defines the 0 K isotherm of polyurea. For the mixture, the left-hand side of (7) is evaluated using the 0 K isotherm parameters. By solving (7) with parameters for the mixture, the Hugoniot of the mixture is obtained. The shock and particle velocities are then obtained using Hugoniot relations corresponding to mass and momentum conservation.

We recall that γ is a parameter coupling the thermal and mechanical properties of a solid and is defined as

$$\gamma = v\frac{\alpha K_T}{C_v}, \tag{9}$$

where, v is the specific volume, $\alpha = \frac{1}{v}\left(\frac{\partial v}{\partial T}\right)_P$ is the volume coefficient of thermal expansion, $K_T = -v\left(\frac{\partial P}{\partial v}\right)_T$ is the isothermal bulk modulus, and $C_v = \frac{1}{v}\left(\frac{\partial E}{\partial T}\right)_v$ is the specific heat capacity at constant volume. It is nearly constant for simple atomic crystals, but exhibits considerable variation with temperature, pressure and phonon frequency for polymers [46, 47]. The variation arises due to the sharply different strengths of interchain and intrachain interactions. At low temperatures, the acoustic phonon modes dominate and the value of γ is high. As the temperature increases, the contribution from the high frequency optical modes increases resulting in a drop in value of γ, which becomes weakly dependent on temperature at normal temperatures [47]. We thus conclude that the assumption that γ_0/v_0 is a material constant independent of shock pressure and temperature (even at 0 K) is only an approximation for polymers.

To calculate γ, we need to first evaluate α, K_T, and C_v. In this work, these parameters were calculated using MD simulation for each shock pressure using the converged shocked configuration. To evaluate the associated derivatives, the temperature or pressure of the shocked configuration was raised and lowered by a small amount, and the system was equilibrated before the requisite properties were calculated by averaging. A linear fit on appropriate parameters yielded the values of the derivatives. In order to calculate α, the temperature was changed by ± 10 K in NPT simulations. To calculate K_T, the pressure was changed by $\pm\Delta P$, where ΔP varied from $10 - 50$ MPa in NPT simulations. For the C_v calculation, the temperature was changed by ± 2.5 K in NVT simulations.

3. Results and discussion

Simulation results are presented in this section. Firstly, the glass transition temperature is calculated from cooling polymer melts. Secondly, the shock response of the two domains is obtained using the multiscale simulation approach discussed earlier. Various features in the shock response of the domains are discussed. Finally, the shock Hugoniots of the two domains are combined to obtain the shock Hugoniot of polyurea, which shows excellent agreement with experimental data. Note that we have used large simulation cells to be able to sample large volume of phase space as well as because it is needed to simulate low pressure shock. However, since we have used only one simulation cell for each domain, the effect of sample variability on the results could not be quantified.

3.1. Glass transition temperature

While cooling the equilibrated melt, the hard phase exhibits a glass transition at 600 K and the soft phase at 312 K, Figure 4. T_g of Poly(tetramethylene oxide) (PTMO), to which T_g of the simulation cell made of soft domain molecules should be compared, is $\sim$ 189 K at experimental cooling rate. At the cooling rate employed in MD simulation, Williams-Landel-Ferry (WLF) equation [48] suggests that T_g of PTMO will shift to 286 K (see Appendix A). T_g obtained from the simulation is reasonably close to the cooling rate corrected T_g of PTMO. The small difference may be arising because we have used the universal WLF constants in the calculation, which may be slightly different from the WLF constants for PTMO. Furthermore, some crystallization also takes place during cooling which is not accounted in the calculation. For the simulation cell consisting of hard domain molecules also, T_g has been corrected using the universal WLF constants. After correction, it is $\sim$ 518 K (see Appendix A), much higher than the room temperature as suggested in the literature [2].

3.2. Shock response of the two domains

From the multiscale shock simulation, we obtain the shock Hugoniot of the two domains of polyurea. To understand the material response at weak shock conditions, typically inaccessible in NEMD simulation, we have performed simulations at shock pressure as low as 0.15 GPa. Figure 5 shows the $u_s - u_p$ plot for the two domains. At very low shock velocities, the slope of $u_s - u_p$ curve is higher than the linear part of the curve at high velocities for both domains, a feature that is typical of polymers. As a consequence, the wave speed in polymers at zero pressure is typically lower than that obtained by extrapolating the linear response at high shock velocities [43]. A curved transition zone is observed between the two linear regimes, though the transitions are qualitatively distinct for both domains. In the soft domain the transition is effected by a smooth curve. By contrast, in the hard domain the transition is so sharp that it resembles a jump in u_p at $u_s \approx 2.65$ km/s. This feature is similar to that observed experimentally in $u_s - u_p$ curve for polymethyl methacrylate (PMMA) [49]. The transition in Hugoniot at low pressure is attributed to contrasting stiffness of bonded interactions and pair interactions that results in pair interaction dominated response at low shock pressures [50]. As the shock pressure

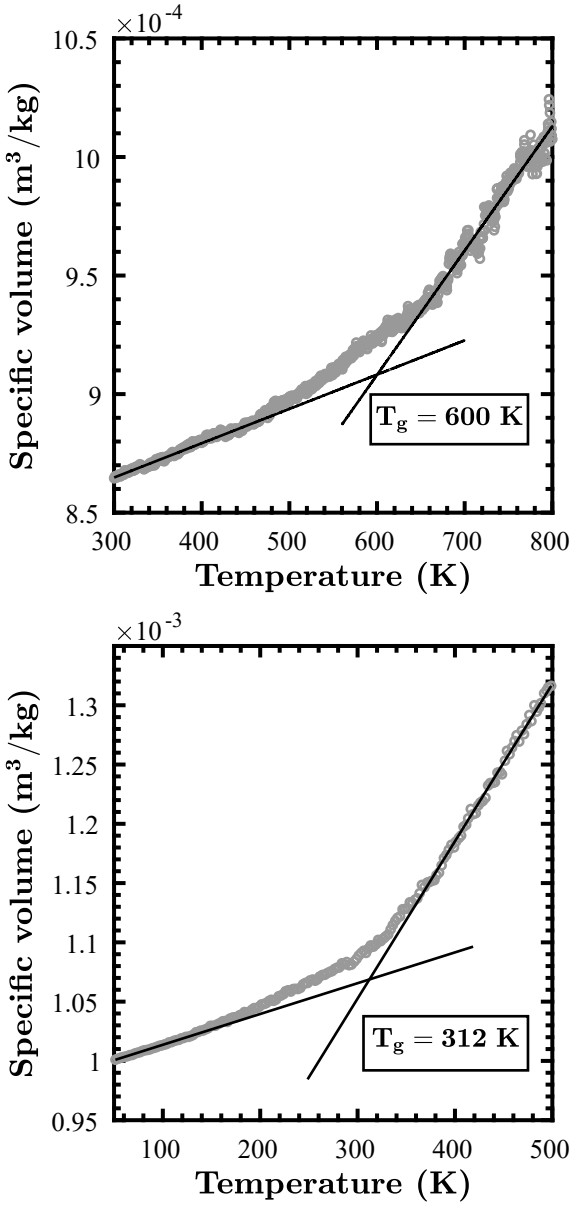

Figure 4: Glass transition in the hard domain (top) and the soft domain (bottom).

increases further, all the interactions contribute to shock response [50], also observed from the variation of energy with shock pressure in Figure 10, resulting in a change in the slope of Hugoniot. Barker *et al.* [49] have suggested that plastic deformation also contributes to the curvature in $u_s - u_p$ curve, however it has not been explored here. It should be noted that low pressure phase transitions are also known to lead to transitions in Hugoniot, as observed in teflon [51], but are not likely to contribute in the case of polyurea due to its amorphous nature.

The slope of the $u_s - u_p$ curve is always lower for the hard domain than for the soft domain, though the magnitude of particle velocity at a given shock velocity is higher. Moreover, at a given shock pressure below 1.62 GPa the shock velocity in the hard domain is larger than that in the soft domain. The trend is reversed above this shock pressure. The particle velocity in the soft domain is always larger.

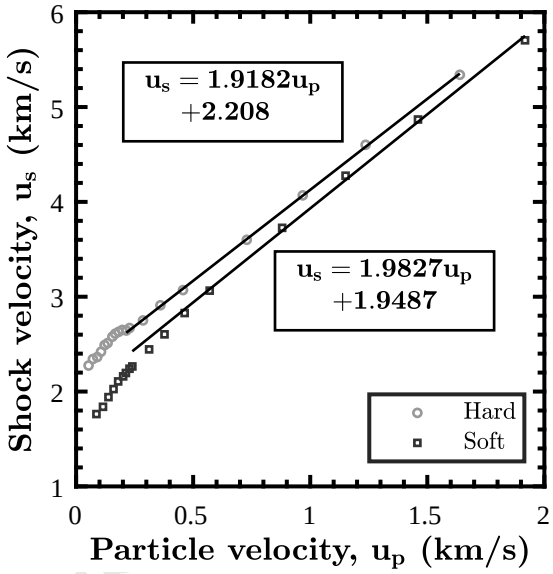

Figure 5: Shock velocity *vs* particle velocity curves for the two domains along with linear fits.

The volumetric compression in the hard domain is smaller than in the soft domain, Figure 6. This difference is expected since the soft domain is above its T_g and compliant, whereas the hard domain is below its T_g and stiff. The low pressure transition clearly visible in $u_s - u_p$ plot is not as obvious in this plot.

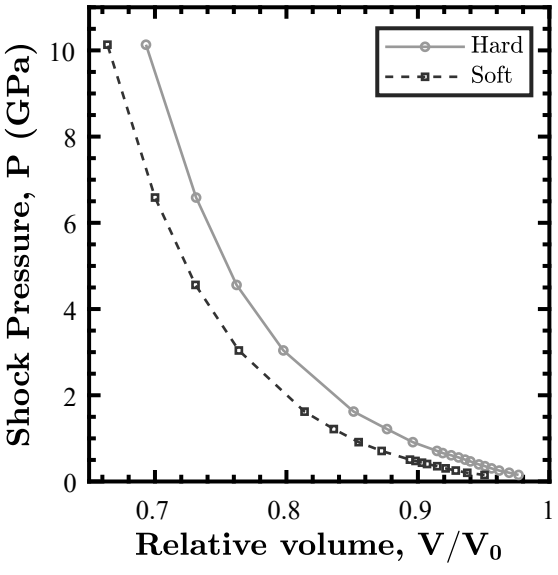

Figure 6: Shock pressure *vs* relative volume curves for the two domains.

The shock simulation also predicts a temperature rise behind the shock front, Figure 7. At a relative volume above

0.85, the soft domain registers a slightly higher rise in temperature due to shock compression, cf. inset in Figure 7. Below 0.85, the hard domain shows a larger rise in temperature. However, at a given shock pressure the soft domain always has a higher rise in temperature.

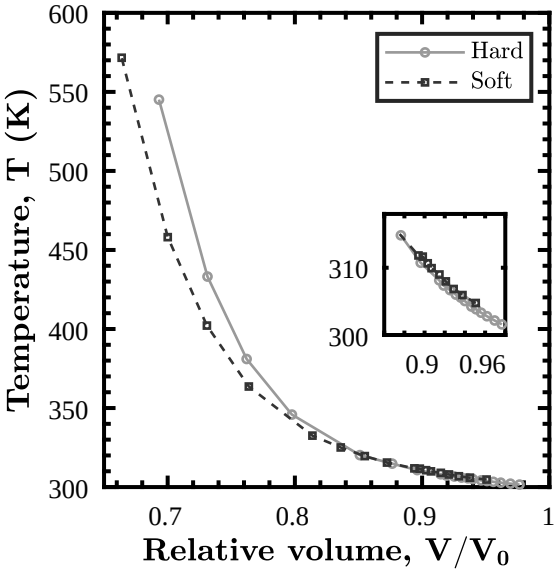

Figure 7: Temperature rise due to shock compression in the two domains.

3.3. Shock-induced structural changes

In order to investigate shock-induced structural changes, particularly in the hard domain, we plot the radial distribution functions of hydrogen atoms surrounding oxygen atoms in urea and ether, and aromatic carbon atoms at different shock pressures, Figure 8. Hydrogen atoms in urea (electropositive) surrounding oxygen atoms in urea and ether (electronegative) can form hydrogen bonds, which are conjectured to contribute to shock energy absorption and dispersion. The first peak in g_{O-H}, Figure 8, corresponds to an intermolecular arrangement of the two groups of atoms, part of which form hydrogen bonds. In the uncompressed state, the peak is located at $r = 1.9$ Å, the distance between the oxygen and hydrogen atoms. The location of the peak decreases with increasing shock strength, as expected from the increase in density. The peak height also decreases, pointing to disruption and breaking of hydrogen bonds. The second sharp peak corresponds to intramolecular oxygen and hydrogen atoms within a urea group.

From the g_{CA-CA} plot in Figure 8, two observations can be made. Firstly, the second peak shows a considerable rise with increasing shock strength. This may arise from bending and twisting around the central aliphatic carbon atom in a hard domain molecule, which brings phenyl rings closer. Secondly, the spikes in the curve corresponding to the uncompressed state, which arise from regular arrangement of carbon atoms within phenyl rings, diminish and finally disappear as the shock strength increases. This points to a considerable disruption in the arrangement of rings in the hard domain as well as distortion of the rings themselves. To confirm ring distortion, we calculated the smallest singular value of a matrix defined by the components of vectors connecting atoms of the ring. In the case of no distortion, this singular value is zero. We find that the statistical average of the smallest singular value of each ring in a simulation cell over time increases with increasing shock pressure, confirming the increasing ring distortion. Open arrangements of atoms such as rings break to accommodate more atoms as shock compression increases [43]. Also, Kovarskii [44] points out that stronger C − C bonds are more prone to breaking than relatively weak C − H bonds. The distortion we observe may thus be a precursor to the breaking of C − C bonds

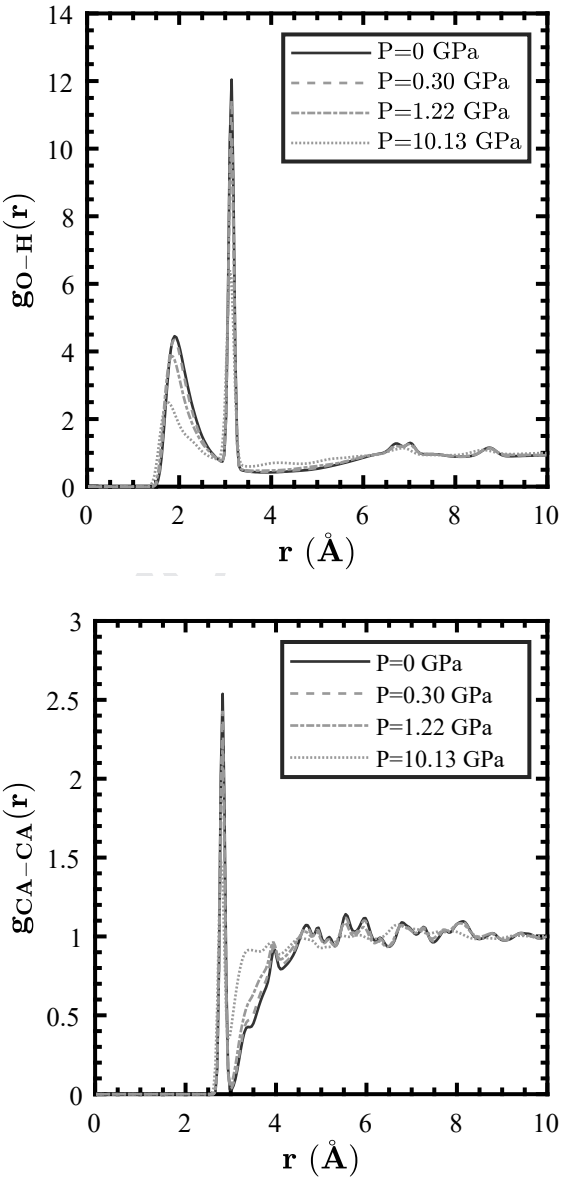

Figure 8: Radial distribution function plotted for hydrogen atoms around an oxygen atom (top), and aromatic carbon atoms (bottom) in the hard domain.

in phenyl rings at higher shock strengths as temperature and pressure reach very high values.

Since the breaking of hydrogen bonds in the hard domain is believed to contribute to shock energy absorption, we track the hydrogen bonds per molecule at different shock pressures. Defining hydrogen bonds requires information on electron density. Since this information is not available in a classical MD simulation, geometric criteria are used instead. We specifically use the criterion that the distance been hydrogen bonded O ⋯ H pairs be less than 2.9 Å, the location of the first minimum in the RDF of O ⋯ H pair, Figure 8, and the angle defined by N − H ⋯ O be greater than 140°. Figure 9 shows a decrease in hydrogen bonding per hard domain molecule due to disruption of the hydrogen bond arrangement. Importantly, the decrease is sharper at low shock pressure.

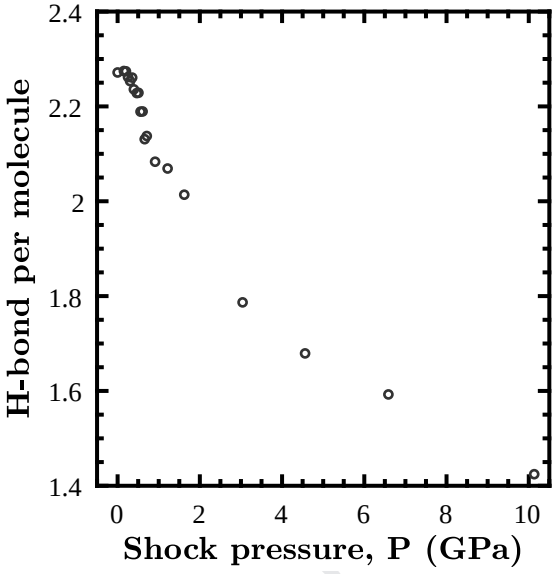

Figure 9: Hydrogen bond per hard domain molecule plotted as a function of shock pressure.

We also examined energies associated with different interactions, Figure 10. We find that the pair energy shows the sharpest increase with increasing shock pressure. Also, the response at small shock pressures is dominated by intermolecular interaction, as argued in [50]. Interestingly, bond and angle energies decrease to a shallow minimum at 3 GPa in the hard domain and at 1.5 GPa in the soft domain, before increasing again. At higher shock pressures, dihedral energy shows the steepest increase with increasing shock pressure after pair energy in the hard domain. In the soft domain, the angular energy shows the steepest increase after pair energy. These differences suggest that different molecular-level mechanisms underlie the shock response of the two domains.

3.4. Hugoniot of polyurea

We now use the mixture rule described in Section 2.3 to estimate the Hugoniot of polyurea. In polyurea P1000,

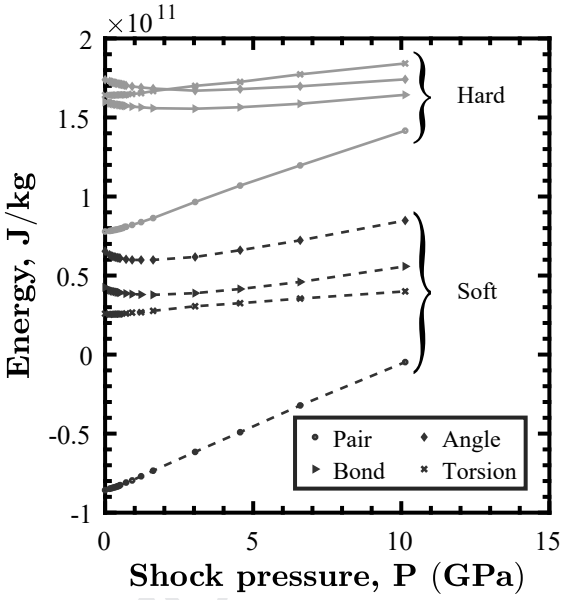

Figure 10: The variation of the energies of different interactions with shock pressure in the two domains.

the hard domain is nominally 35% by weight [13, 22]. The parameter γ for the two domains shows a weak dependence on shock pressure and varies between $0.15-0.55$. Averaging over different shock pressures, we obtain an average value of γ of 0.3006 for the hard domain and 0.3879 for the soft domain. Likewise, we compute an average value of γ_0/v_0 of 0.4054 g/cm^3 for the hard domain and 0.4303 g/cm^3 for the soft domain. To solve (7), we need to calculate slope of the Hugoniot curves for the two domains. To that end, we fit polynomials of degree four to the hard and soft domain Hugoniots.

Figure 11 and Figure 12 show the $u_s - u_p$ and pressure-compression curves for polyurea and compare the results with available experimental data. An excellent agreement is observed. Furthermore, our results fill the gap between $4 - 10$ GPa in the experimental data. At high shock pressure, the computed results and data from Pacheco *et al.* [24] exhibit similar volume compression. However, some discrepancy between shock and particle velocities is observed. This discrepancy may result from differences in sample density. The density of polyurea in our model is 0.996 g/cm^3, in contrast to 1.098 g/cm^3 in Mock *et al.* [22] and 1.134 g/cm^3 in Pacheco *et al.* [24].

4. Concluding remarks

In order to understand the molecular-level mechanisms responsible for shock mitigation in polyurea, we have studied the shock response of the hard and the soft domains independently using molecular dynamics (MD) simulations. Our study focuses on the response in the range from weak shock pressure, typically inaccessible in NEMD simulations, to moderately high shock pressure. Both domains exhibit atypical behavior at low pressure, known for polymers. This

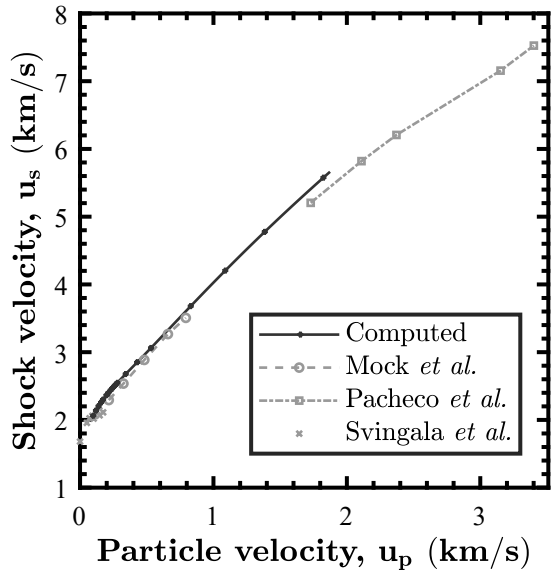

Figure 11: Shock velocity *vs* particle velocity curves for polyurea obtained using a mixture rule and compared with experimental data.

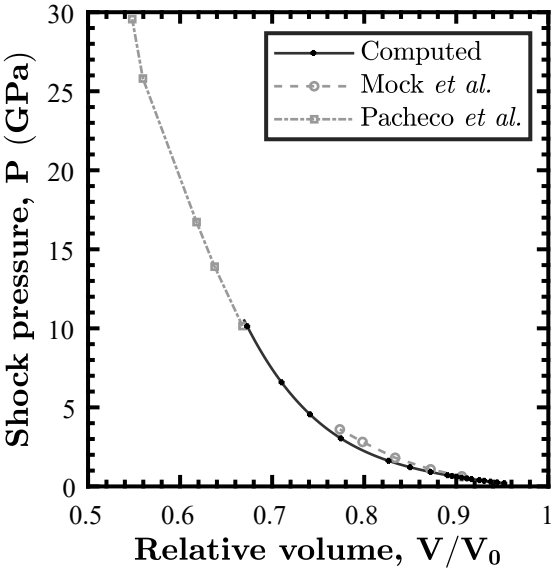

Figure 12: Shock pressure *vs* relative volume curves for polyurea obtained using a mixture rule and compared with experimental data.

atypical behavior may be attributed to the contrast in interchain and intrachain interaction in polymers, as well as to plastic deformation. At a given shock pressure, the hard domain shows less compression and a relatively smaller rise in temperature relative to the soft domain. However, it shows considerable hydrogen bond breaking. RDF of aromatic carbons, geometry analysis and trends in energy distribution suggest severe disruption in the arrangement of phenyl rings and distortion in the ring structure at high shock pressure, which may be conjectured as a precursor to ring breaking at even higher shock pressures.

Finally, using a mixture rule, the shock Hugoniot of the two domains can be combined to obtain the shock response of polyurea. An excellent agreement between simulation and experiment is recorded, which tends to validate the method of analysis. Furthermore, the calculations fill in a range of shock pressures in which experimental shock data are not available.

The model presented here does not take interfacial properties into account. However, the experiments by Castagana *et al.* [13, 15] suggest substantial phase mixing near the interface. An objective evaluation of interfacial effects on shock mitigation remains a challenge for further study.

A. Effect of cooling rate on T_g

Cooling rate in MD simulation is orders of magnitude faster than the experimental cooling rate used in the measurement of T_g. WLF equation [48]

$$\log(a_T) = \frac{-C_1(T - T_g)}{C_2 + T - T_g}, \tag{10}$$

where a_T is the shift factor, C_1 and C_2 are the material dependent constants, and T is the temperature, can also used to estimate the change in T_g due to a change in cooling rate [52]. In this case,

$$\log(a_T) = \log\left(\frac{\dot{T}_r}{\dot{T}}\right) = \frac{-C_1(T'_g - T_g)}{C_2 + T'_g - T_g}, \tag{11}$$

where $\dot{T}$ is the applied cooling rate, $\dot{T}_r$ is the experimental cooling rate, and T'_g is the glass transition temperature at the applied cooling rate. (11) can be rewritten to obtain an expression for the change in T_g:

$$\Delta T_g = T'_g - T_g = \frac{-C_2 \log\left(\frac{\dot{T}_r}{\dot{T}}\right)}{C_1 + \log\left(\frac{\dot{T}_r}{\dot{T}}\right)}. \tag{12}$$

For linear amorphous polymers, the constants in the above equation are close to the universal WLF constants ($C_1 = 17.44$, and $C_2 = 51.6$ K) [52]. On substituting $\dot{T} = 25 \times 10^9$ K/s, the cooling rate used in MD simulation of the cell of soft domain molecules, and $\dot{T}_r = 0.1$ K/s, we obtain $\Delta T_g = 97$ K. Assuming the universal WLF constants to be valid for hard domain as well, and substituting $\dot{T} = 5 \times 10^9$ K/s, we obtain $\Delta T_g = 82$ K.

References

[1] D. J. Primeaux, Polyurea elastomer technology: history, chemistry & basic formulating techniques, Primeaux Associates LLC (2004) 1–20.

[2] R. Bogoslovov, C. Roland, R. Gamache, Impact-induced glass transition in elastomeric coatings, Applied physics letters 90 (2007) 221910.

[3] T. Jiao, R. Clifton, Measurement of the response of an elastomer at pressures up to 9 gpa and shear-rates of 105–106s- 1, in: Journal of Physics: Conference Series, volume 500, IOP Publishing, p. 112036.
[4] P. Mott, C. Giller, D. Fragiadakis, D. Rosenberg, C. Roland, Deformation of polyurea: where does the energy go?, Polymer 105 (2016) 227–233.
[5] J. Porter, R. Dinan, M. Hammons, K. Knox, Polymer coatings increase blast resistance of existing and temporary structures., Amptiac Quarterly 6 (2002) 47–52.
[6] S. M. Walsh, B. R. Scott, D. M. Spagnuolo, The development of a hybrid thermoplastic ballistic material with application to helmets, Technical Report, ARMY RESEARCH LAB ABERDEEN PROVING GROUND MD, 2005.
[7] Y. A. Bahei-El-Din, G. J. Dvorak, O. J. Fredricksen, A blast-tolerant sandwich plate design with a polyurea interlayer, International Journal of Solids and Structures 43 (2006) 7644–7658.
[8] S. A. Tekalur, A. Shukla, K. Shivakumar, Blast resistance of polyurea based layered composite materials, Composite Structures 84 (2008) 271–281.
[9] N. Iqbal, M. Tripathi, S. Parthasarathy, D. Kumar, P. Roy, Polyurea coatings for enhanced blast-mitigation: a review, RSC advances 6 (2016) 109706–109717.
[10] J. Pathak, J. Twigg, K. Nugent, D. Ho, E. Lin, P. Mott, C. Robertson, M. Vukmir, T. Epps Iii, C. Roland, Structure evolution in a polyurea segmented block copolymer because of mechanical deformation, Macromolecules 41 (2008) 7543–7548.
[11] R. Rinaldi, M. Boyce, S. Weigand, D. Londono, M. Guise, Microstructure evolution during tensile loading histories of a polyurea, Journal of Polymer Science Part B: Polymer Physics 49 (2011) 1660–1671.
[12] M. Grujicic, T. He, B. Pandurangan, F. Svingala, G. Settles, M. Hargather, Experimental characterization and material-model development for microphase-segregated polyurea: an overview, Journal of Materials Engineering and Performance 21 (2012) 2–16.
[13] A. M. Castagna, A. Pangon, T. Choi, G. P. Dillon, J. Runt, The role of soft segment molecular weight on microphase separation and dynamics of bulk polymerized polyureas, Macromolecules 45 (2012) 8438–8444.
[14] T. Choi, D. Fragiadakis, C. M. Roland, J. Runt, Microstructure and segmental dynamics of polyurea under uniaxial deformation, Macromolecules 45 (2012) 3581–3589.
[15] A. M. Castagna, A. Pangon, G. P. Dillon, J. Runt, Effect of thermal history on the microstructure of a poly (tetramethylene oxide)-based polyurea, Macromolecules 46 (2013) 6520–6527.
[16] G. Tsagaropoulos, A. Eisenburg, Direct observation of two glass transitions in silica-filled polymers. implications to the morphology of random ionomers, Macromolecules 28 (1995) 396–398.
[17] M. Grujicic, J. Snipes, S. Ramaswami, R. Galgalikar, J. Runt, J. Tarter, Molecular-and domain-level microstructure-dependent material model for nano-segregated polyurea, Multidiscipline Modeling in Materials and Structures (2013).
[18] J. Lee, V. M. Lau, Y. Ren, C. M. Evans, J. S. Moore, N. R. Sottos, Effect of polymerized ionic liquid structure and morphology on shock-wave energy dissipation, ACS Macro Letters 8 (2019) 535–539.
[19] S. S. Sarva, S. Deschanel, M. C. Boyce, W. Chen, Stress–strain behavior of a polyurea and a polyurethane from low to high strain rates, Polymer 48 (2007) 2208–2213.
[20] T. Jiao, R. Clifton, S. Grunschel, Pressure-sensitivity and constitutive modeling of an elastomer at high strain rates, in: AIP Conference Proceedings, volume 1195, American Institute of Physics, pp. 1229–1232.
[21] M. Alkhader, W. Knauss, G. Ravichandran, A new shear-compression test for determining the pressure influence on the shear response of elastomers, Experimental mechanics 52 (2012) 1151–1161.
[22] W. Mock Jr, S. Bartyczak, G. Lee, J. Fedderly, K. Jordan, Dynamic properties of polyurea 1000, in: AIP Conference Proceedings, volume 1195, American Institute of Physics, pp. 1241–1244.
[23] F. Svingala, M. Hargather, G. Settles, Optical techniques for measuring the shock hugoniot using ballistic projectile and high-explosive shock initiation, International journal of impact engineering 50 (2012) 76–82.
[24] A. Pacheco, R. Gustavsen, T. Aslam, B. Bartram, Hugoniot based equation of state for solid polyurea and polyurea aerogels, in: AIP Conference Proceedings, volume 1793, AIP Publishing LLC, p. 120029.
[25] T. C. Ransom, M. Ahart, R. J. Hemley, C. M. Roland, Vitrification and density scaling of polyurea at pressures up to 6 gpa, Macromolecules 50 (2017) 8274–8278.
[26] T. C. Ransom, M. Ahart, R. J. Hemley, C. M. Roland, Acoustic properties and density of polyurea at pressure up to 13.5 gpa through brillouin scattering spectroscopy, Journal of Applied Physics 123 (2018) 195102.
[27] D. Fragiadakis, R. Gamache, R. Bogoslovov, C. Roland, Segmental dynamics of polyurea: effect of stoichiometry, Polymer 51 (2010) 178–184.
[28] M. Grujicic, R. Yavari, J. Snipes, S. Ramaswami, J. Runt, J. Tarter, G. Dillon, Molecular-level computational investigation of shock-wave mitigation capability of polyurea, Journal of Materials Science 47 (2012) 8197–8215.
[29] M. Grujicic, J. Snipes, S. Ramaswami, R. Yavari, M. Ramasubramanian, Meso-scale computational investigation of shock-wave attenuation by trailing release wave in different grades of polyurea, Journal of materials engineering and performance 23 (2014) 49–64.
[30] J. Qiao, A. V. Amirkhizi, K. Schaaf, S. Nemat-Nasser, G. Wu, Dynamic mechanical and ultrasonic properties of polyurea, Mechanics of Materials 43 (2011) 598–607.
[31] B. Arman, A. S. Reddy, G. Arya, Viscoelastic properties and shock response of coarse-grained models of multiblock versus diblock copolymers: insights into dissipative properties of polyurea, Macromolecules 45 (2012) 3247–3255.
[32] M. Grujicic, R. Yavari, J. Snipes, S. Ramaswami, T. Jiao, R. Clifton, Experimental and computational study of the shearing resistance of polyurea at high pressures and high strain rates, Journal of Materials Engineering and Performance 24 (2015) 778–798.
[33] K. Yao, Z. Liu, T. Li, B. Guo, Z. Zhuang, Mesoscale structure-based investigation of polyurea dynamic modulus and shock-wave dissipation, Polymer (2020) 122741.
[34] M. Grujicic, J. Snipes, S. Ramaswami, R. Yavari, J. Runt, J. Tarter, G. Dillon, Coarse-grained molecular-level analysis of polyurea properties and shock-mitigation potential, Journal of materials engineering and performance 22 (2013) 1964–1981.
[35] S. Heyden, M. Ortiz, A. Fortunelli, All-atom molecular dynamics simulations of multiphase segregated polyurea under quasistatic, adiabatic, uniaxial compression, Polymer 106 (2016) 100–108.
[36] R. McQueen, S. Marsh, J. Taylor, J. Fritz, W. Carter, High-velocity impact phenomena, Academic Press, New York, 1970) p 244 (1970).
[37] S. Plimpton, Fast parallel algorithms for short-range molecular dynamics, Journal of Computational Physics 117 (1995) 1 – 19.
[38] W. L. Jorgensen, J. Tirado-Rives, The opls [optimized potentials for liquid simulations] potential functions for proteins, energy minimizations for crystals of cyclic peptides and crambin, Journal of the American Chemical Society 110 (1988) 1657–1666.
[39] W. L. Jorgensen, D. S. Maxwell, J. Tirado-Rives, Development and testing of the opls all-atom force field on conformational energetics and properties of organic liquids, Journal of the American Chemical Society 118 (1996) 11225–11236.
[40] J.-B. Maillet, M. Mareschal, L. Soulard, R. Ravelo, P. S. Lomdahl, T. C. Germann, B. L. Holian, Uniaxial hugoniostat: A method for atomistic simulations of shocked materials, Physical Review E 63 (2000) 016121.
[41] E. J. Reed, L. E. Fried, J. Joannopoulos, A method for tractable dynamical studies of single and double shock compression, Physical review letters 90 (2003) 235503.
[42] R. Ravelo, B. Holian, T. Germann, P. Lomdahl, Constant-stress hugoniostat method for following the dynamical evolution of shocked matter, Physical Review B 70 (2004) 014103.

[43] W. Carter, S. Marsh, Hugoniot equation of state of polymers, Technical Report, Los Alamos National Lab., NM (United States), 1995.
[44] A. L. Kovarskii, High-pressure chemistry and physics of polymers, CRC Press, 1994.
[45] M. A. Meyers, Dynamic behavior of materials, John wiley & sons, 1994.
[46] J. G. Curro, Calculation of grüneisen parameters of polymers, The Journal of Chemical Physics 58 (1973) 374–380.
[47] Y. K. Godovsky, Thermophysical properties of polymers, Springer Science & Business Media, 2012.
[48] J. D. Ferry, Viscoelastic properties of polymers, John Wiley & Sons, 1980.
[49] L. M. Barker, R. Hollenbach, Shock-wave studies of pmma, fused silica, and sapphire, Journal of Applied Physics 41 (1970) 4208–4226.
[50] D. J. Pastine, P, v, t equation of state for polyethylene, The Journal of Chemical Physics 49 (1968) 3012–3022.
[51] A. Champion, Shock compression of teflon from 2.5 to 25 kbar-evidence for a shock-induced transition, Journal of Applied Physics 42 (1971) 5546–5550.
[52] A. Soldera, N. Metatla, Glass transition of polymers: Atomistic simulation versus experiments, Physical Review E 74 (2006) 061803.

- Shock response of the phase segregated domains have been studied independently.
- The response of polyurea is obtained by combining the responses of the two domains.
- Computed shock Hugoniot of polyurea shows excellent agreement with experiments.
- Hard domain mitigates shock by hydrogen bond breaking and aromatic ring distortion.

Declaration of interests

☒ The authors declare that they have no known competing financial interests or personal relationships that could have appeared to influence the work reported in this paper.

☐The authors declare the following financial interests/personal relationships which may be considered as potential competing interests: